

MonoCT: Overcoming Monocular 3D Detection Domain Shift with Consistent Teacher Models

Johannes Meier^{*,1,2,3}, Louis Inchingolo^{*,2}, Oussema Dhaouadi^{1,2,3},
 Yan Xia^{2,3,†}, Jacques Kaiser¹, Daniel Cremers^{2,3}
¹ DeepScenario ² TU Munich ³ Munich Center for Machine Learning

Abstract—We tackle the problem of monocular 3D object detection across different sensors, environments, and camera setups. In this paper, we introduce a novel unsupervised domain adaptation approach, MonoCT, that generates highly accurate pseudo labels for self-supervision. Inspired by our observation that accurate depth estimation is critical to mitigating domain shifts, MonoCT introduces a novel Generalized Depth Enhancement (GDE) module with an ensemble concept to improve depth estimation accuracy. Moreover, we introduce a novel Pseudo Label Scoring (PLS) module by exploring inner-model consistency measurement and a Diversity Maximization (DM) strategy to further generate high-quality pseudo labels for self-training. Extensive experiments on six benchmarks show that MonoCT outperforms existing SOTA domain adaptation methods by large margins ($\sim 21\%$ minimum for AP Mod.) and generalizes well to car, traffic camera and drone views.

I. INTRODUCTION

Autonomous driving systems depend on robust perception to navigate safely, making accurate 3D object detection essential for identifying traffic participants (e.g., vehicles) [1]. Although LiDAR-based detectors [2], [3], [4], [5] provide high precision due to the accurate depth measurement, they are costly and require complex infrastructure. 3D object detection from monocular cameras offers a more affordable and accessible alternative, drawing increasing attention in the robotics and computer vision communities [6].

Recent monocular 3D detectors work on the RGB images captured from the cameras mounted on autonomous vehicles. With the development of *Cooperative Vehicle-Infrastructure Systems* (CVIS), traffic cameras and drone data are becoming increasingly important [7], [8], [9]. Traffic cameras, fixed in position, can improve scene understanding [7], [10], while drones can capture occlusion-free trajectory data, that can be used to enhance planning and prediction models for autonomous driving [11], [12]. It is therefore essential to develop the capability to perform monocular 3D detection across car-traffic-drone views, as shown in Fig. 1 (Top).

We find that current monocular 3D detection methods suffer performance drops when used with different sen-

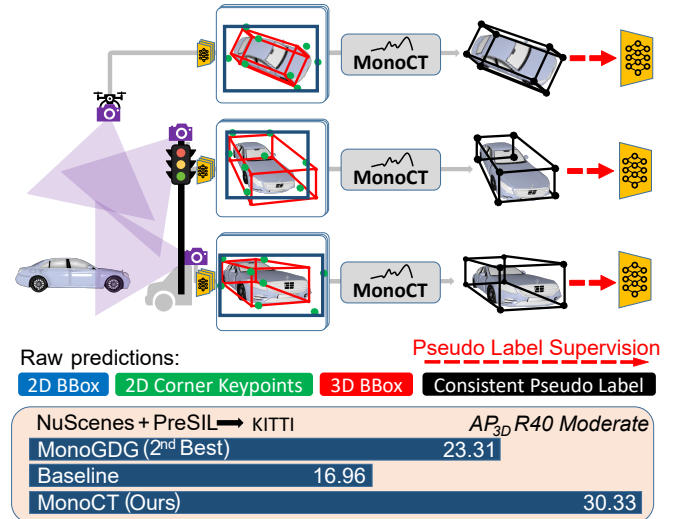


Fig. 1: MonoCT generates precise pseudo labels to overcome domain shift in monocular 3D object detection, utilizing inner-model and multi-model consistency. These labels are then used to self-supervise the detector. Our approach accommodates car-traffic-drone views and greatly improves the current SOTA methods.

sors, weather conditions, geographic locations, annotation styles, or traffic densities. For instance, CoBEV [13] and BEVFormer [14]) exhibit performance drops of 57.4% and 48.7%, respectively, when applied in unknown versus known camera locations (*cf.* Rope3D Homologous vs. Rope3D Heterologous) [8], [13]. While domain adaptation has been widely studied for LiDAR data [15], [16], [17], [18], to date, a few monocular 3D detection methods have been proposed for domain shift in different environments and camera views. MonoGDG [19] and DGMono3D [20] focus on sensor alignment, calibrating the *field of view* (FOV) between source and target domains. STMono3D [21] and MonoTTA [22] explore a self-training strategy and simple filter schemes for pseudo-label selection. However, they overlook the importance of depth and fail to identify high-quality pseudo labels. Recent Mix-Teaching [23] explores a semi-supervised way to train an ensemble of teacher models. However, it selects pseudo labels without considering the inner-model depth consistency. To overcome these limitations, we propose a novel network, named MonoCT, to address the Monocular 3D detection domain shift across car-traffic-drone views with Consistent

*Equal Contribution, † Corresponding author.

TUM: j.meier@tum.de, firstname.lastname@tum.de
 DeepScenario: firstname@deepscenario.com

This work is a result of the joint research project STADT.up. The project is supported by the German Federal Ministry for Economic Affairs and Climate Action (BMWK), based on a decision of the German Bundestag. The author is solely responsible for the content of this publication. This work was also supported by the ERC Advanced Grant SIMULACRON. We acknowledge ChatGPT for assistance with polishing and grammar checks.

Teacher (CT) models.

As pointed out in [24], [25], [26], the main challenge in monocular 3D object detection lies in accurately predicting depth. Inspired by that, we first propose a novel ensemble-based method to improve the quality of depth estimation. Specifically, we generate 48 auxiliary depth estimates using predictions of 2D keypoints and 2D bounding boxes. These are then consolidated into a single, outlier-resistant prediction using kernel density estimation. We then propose a Pseudo Label Scoring (PLS) module to evaluate the quality of pseudo-labels by leveraging both 2D/3D consistency and inner-model depth consistency. Another observation is that cars with orientations driving forward, backward, left, or right relative to the camera are selected more frequently as pseudo labels. To avoid oversampling and bias toward simpler cases, we enhance the generation of highly accurate and diverse pseudo-labels by introducing Diversity Maximization.

To summarize, the key contributions of this work are:

- We focus on the fairly understudied problem of monocular 3D object detection across car-traffic-drone views, to overcome the domain shift challenges.
- We propose a novel *Generalized Depth Enhancement* (GDE) method that can accurately estimate depth and generalize effectively to car-traffic-drone perspectives.
- We propose a *Pseudo Label Scoring* (PLS) module and show that it can predict the overlap of the top pseudo labels with ground truth more accurately than previous scoring methods.
- We design a *Diversity Maximization* (DM) strategy to avoid model bias towards simpler configurations when selecting pseudo labels.
- We conduct extensive experiments on the six widely used benchmarks, NuScenes, Lyft, KITTI, PreSIL, Rope3D, and CDrone, including cross-dataset, synthetic-to-real, and weather condition domain shifts. Experiments demonstrate that the proposed MonoCT outperforms the state-of-the-art methods.

II. RELATED WORKS

Monocular 3D Object Detection Recent monocular 3D detection research has centered on egocentric car-view datasets like KITTI [27] and Waymo [28], with depth estimation being a key challenge [24], [29], [25]. While LiDAR point clouds improve depth accuracy [30], [31], [1], this dependency limits applicability to datasets without LiDAR [8], [7]. DEVIANT [32] and MonoLSS [33] explore depth-equivariant backbones and feature relevance scoring to enhance depth without LiDAR. Yan et al. [25] showed that ensemble-based depth estimation improves detection accuracy. Several works use 2D keypoints to aid depth estimation: MonoFlex [24] and MonoDDE [26] derive depth from keypoints, while RTM3D [34] and MonoCon [35] leverage keypoints for object positioning and generalization. However, these methods are limited to car views due to assumptions like a single y-axis rotation [9]. In contrast, our MonoCT generalizes across drones and traffic views.

Domain adaptation for LiDAR based 3D object detection

Recent research in domain adaptation for 3D object detection has primarily focused on LiDAR-based detectors. Current methods address domain shift via sensor alignment [15], [36], feature alignment [36], [37], student-teacher training [16], [38], [39], [40], [37], and temporal consistency [41], [42], [17]. MS3D [43] and MS3D++ [41] use kernel density estimation (KDE) to combine predictions from multiple teacher models trained on distinct source domains. While we also employ a KDE, we apply it to depth estimation. Image-based detectors like BEVUDA [44] and MonoTDP [45] incorporate LiDAR during training to handle domain shifts, but we avoid this dependency since not all monocular datasets include LiDAR [8].

Domain adaptation for monocular 3D object detection

Current cross-dataset adaptation methods normalize camera intrinsics to handle varying parameters [46], [20], [21], [19]. Zheng *et al.* [46] align the ego-frame and use extrinsics-aware RoI sizes, while DGMono3D [20] and MonoGDG [19] align the FOV between source and target domains, with DGMono3D also utilizing target dataset object dimensions. Similar to STMono3D [21], we leverage unlabeled target data to enhance accuracy, though we show standard 3D detection scores fail to identify high-quality pseudo labels. WARM3D [47] uses weak supervision with 2D bounding box labels and a 2D/3D consistency loss, focusing on traffic views. In this work, we solve domain shifts in all perspectives, including car, traffic camera and drone views. While Mix-Teaching [23] filters based on teacher ensemble agreement, we show that filtering based on inner-model consistency is more effective.

III. METHOD

A. Problem Statement

The task of monocular 3D detection aims to predict 3D bounding boxes (BBoxes) b_1, \dots, b_n of objects from an RGB image I with intrinsics $K \in \mathbb{R}^{3 \times 4}$. Each box b_i is defined by its position (x, y, z) relative to the camera, its dimensions (l, w, h) , its egocentric orientation matrix $R \in SO(3)$, and category $c \in \mathbb{N}$. For unsupervised domain adaptation, we use labeled source domain data $D_s = \{I_j, K_j, \{b_{j,i}\}_{i=1}^{n_j}\}_{j=1}^{M_s}$ and unlabeled target domain data $D_t = \{I'_j, K'_j\}_{j=1}^{M_t}$ to maximize detection performance on the target test set. Fig. 2 shows our MonoCT architecture and will be explained in the following.

B. Baseline

We use the state-of-the-art detector MonoCon [35] with virtual depth [49] (denoted as MCVD) as our baseline. MonoCon estimates offsets from the 2D object center to the projected 3D corner keypoints in pixel space as an auxiliary task. Our MonoCT leverages these additional predictions in Section III-C. Note that this auxiliary task can be easily integrated into other monocular 3D detectors.

Generalization to new camera parameters To handle varying camera intrinsics across domains (*e.g.* Lyft \rightarrow KITTI), we use virtual depth z_t [49] as training target instead

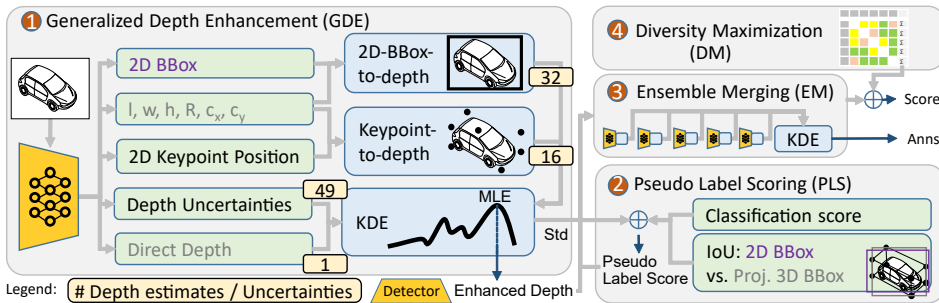


Fig. 2: **Overview of our MonoCT for pseudo label generation:** (1) **GDE**: We convert auxiliary 2D BBox and 2D corner keypoint predictions into depth estimates, which are then merged into a single depth estimate using a *kernel density estimator* (KDE). (2) **PLS**: To identify the most accurate pseudo labels, we assess the standard deviation of the KDE and evaluate 2D/3D BBox consistency. (3) **EM**: We enhance predictions further by employing an ensemble of five teacher models. (4) **DM**: We filter pseudo labels for quality and rotation diversity to optimize self-training.

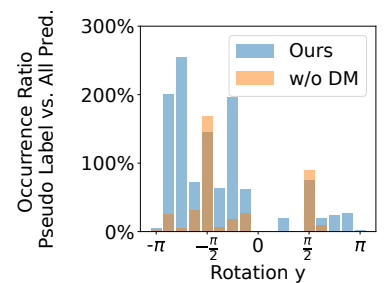


Fig. 3: **Diversity Maximization (DM)**: Without DM, pseudo labels are concentrated at $\pm \frac{\pi}{2}$. With DM, high-quality labels are more evenly distributed across all orientations (Lyft [48] \rightarrow KITTI [27]).

of ground truth depth. The reason is that training MonoCon on the source domain only results in a score of 0 due to intrinsic shifts [21]. We normalize depth with respect to camera intrinsics, with the added benefit of enabling scale augmentation: $z_t = s_{\text{aug}} \cdot \frac{f_{\text{ref}}}{f_{\text{img}}} \cdot z$, where z is the ground truth depth, $\frac{f_{\text{ref}}}{f_{\text{img}}}$ is the ratio of the virtual to actual focal length, and s_{aug} is the scale factor from augmentation. During inference, we unnormalize the depth by computing the inverse. This approach enhances robustness to intrinsic changes and supports scale augmentation during training. The virtual focal length can be set arbitrarily. In our experiments, we set $f_{\text{ref}} = 700$.

Support for $SO(3)$ rotations To effectively handle varying perspectives, our MonoCT predicts $SO(3)$ rotations rather than a single rotation angle using an allocentric orientation representation [9]. To maintain the properties of rotation matrices, we employ Gram-Schmidt orthogonalization. For further details, we refer to Brazil *et al.* [49].

Teacher-student training We leverage unlabeled target domain data through self-training in a teacher-student setup. We train an ensemble of five teacher models (same architecture, different seeds) on the source data and use the model ensemble to identify high-quality pseudo labels. Like Mix-Teaching [23], we paste pseudo labels into empty images using border-cut, MixUp [50], and padding augmentation. To optimize resource efficiency, we perform only a single round of self-training.

C. Generalized Depth Enhancement (GDE)

Here, we introduce a novel method that converts auxiliary 2D predictions into 48 additional depth estimates and combines them into a single, unified estimate. Different from previous methods [24], [25], [26], [51], which are limited to the egocentric car perspective, our method is designed to work with car, traffic, and drone views.

Keypoint-to-depth Our baseline model predicts the 2D corner keypoint coordinates (kp_x^{2D}, kp_y^{2D}) for each BBox as an auxiliary task (*center to keypoint*). As they can also be obtained by projecting the 3D keypoint position

$(kp_x^{3D}, kp_y^{3D}, kp_z^{3D})$ into the image, we have:

$$kp_z^{3D} \cdot [kp_x^{2D}, kp_y^{2D}, 1]^T = K[kp_x^{3D}, kp_y^{3D}, kp_z^{3D}, 1]^T. \quad (1)$$

Solving Eq. (1) for depth yields two estimates for kp_z^{3D} at each corner point, denoted as z_x and z_y :

$$z_x = \frac{f_x \cdot b_x + (c_x - kp_x^{2D}) \cdot b_z}{kp_x^{2D} - a_x} \quad (2)$$

$$z_y = \frac{f_y \cdot b_y + (c_y - kp_y^{2D}) \cdot b_z}{kp_y^{2D} - a_y}, \quad (3)$$

$$\text{with } [b_x, b_y, b_z]^T = R([r_x, r_y, r_z]^T \odot [l, w, h]^T) \quad (4)$$

where (a_x, a_y) denotes the projected 3D object center, R is the egocentric orientation matrix, $[l, w, h]$ is the object dimension, (c_x, c_y) is the principal point, f_x, f_y are the focal lengths, \odot refers to the Hadamard product, and (r_x, r_y, r_z) defines the keypoint location relative to the object with $r_x, r_y \in \{-0.5, 0.5\}$ and $r_z \in \{0, 1\}$. This formulation gives us 16 depth estimates and can be considered a generalization of MonoDDE’s approach [26] to $SO(3)$ rotation.

2D-bounding-box-to-depth Estimating the 2D BBox is generally easier than estimating the 3D BBox. Based on this insight, we use the projected 3D BBox as the target for training the 2D BBox of our detector [9]. Assuming no truncation at the image boundaries, each side of the 2D bounding box must encompass at least one keypoint: one keypoint’s x-coordinate will align with the left side and another with the right, while one keypoint’s y-coordinate will coincide with the top and another with the bottom. Given that there are 8 corner points and 4 potential positions (left, right, bottom, top), there are 32 possible combinations, of which at least 4 are valid. We use this information to obtain depth estimates for each combination using Eq. (2) and Eq. (3).

Depth merging Only a subset of these $16 + 32 = 48$ auxiliary depth estimates will be accurate. *E.g.* consider the case, where we assume the keypoint is on the left side, but it is actually on the right side. In this case, the computed depth

is negative. Instead of hand-designing a complex filtering mechanism, we let the network learn the aleatoric uncertainty that the estimated depth is correct. We add the following loss:

$$\mathcal{L}_{\text{aux}} = \frac{1}{48} \sum_{i=1}^{48} \sqrt{2} \cdot \frac{|\hat{z}_i - z_t|}{\hat{\sigma}_i} + \log \hat{\sigma}_i \quad (5)$$

where \hat{z}_i and $\hat{\sigma}_i$ are the auxiliary depth estimates and implicitly learned uncertainties. Since \hat{z}_i are obtained in closed-form from the network output, we only backpropagate through the uncertainties $\hat{\sigma}_i$.

The output depth is obtained by combining all depth estimates: the 48 estimations and an additional direct depth prediction (49 depth estimates in total). Previous methods have employed the weighted mean, which is equivalent to *weighted box fusion* (WBF) [24], [26], [52]. However, we empirically notice that it is not robust against outliers. Instead, we use kernel density estimation to merge the predictions. A KDE can generate a continuous density function from sample points without requiring any additional parameters about the distribution of these points. For simplicity, we use a Gaussian kernel and infer the bandwidth parameter h with Silverman’s rule of thumb [53]. We parametrize the points with our predicted depth values and set the weight to the exponential inverse uncertainty $w_i = \frac{\exp \hat{\sigma}_i^{-1}}{\sum_j^{49} \exp \hat{\sigma}_j^{-1}}$:

$$\hat{f}_h(z) = \sum_{i=1}^{49} w_i \frac{1}{\sqrt{2\pi}h^2} \exp \left(-\frac{(z - z_i)^2}{2h^2} \right). \quad (6)$$

We perform *maximum likelihood estimation* (MLE) on the KDE density to infer our merged depth because it is more robust to noise than alternatives like WBF. This method ensures a high likelihood when multiple high-confidence depth predictions are closely grouped. In contrast, outliers, which generally have low confidence and few neighboring points, contribute to lower likelihood values.

D. Pseudo Label Scoring (PLS)

Selecting only high-quality pseudo labels ensures the model learns reliable patterns from the target domain. While the default MonoCon [35] score (class score times depth certainty) is adequate for evaluating overall prediction quality, it is not ideal for identifying the small subset of high-quality labels needed for self-training. We propose a new pseudo label score $s_{\text{pseudo}} = (s_{\text{cls}} + s_{\text{KDE}} + s_{2D/3D})/3$, where s_{cls} is the default class score of MonoCon [35], $s_{\text{KDE}} = \exp(-\text{STD}_{\text{KDE}}(z))$ is the negative exponential of the KDE’s standard deviation, and $s_{2D/3D}$ is the *intersection over union* (IoU) between the predicted 2D BBox and the projected 3D BBox. This new score emphasizes model consistency: when multiple high-confidence depth predictions are close together (high consistency), s_{KDE} is high, whereas when predictions are far apart (low consistency), s_{KDE} is low.

E. Ensemble Merging (EM)

Inspired by [43], [41], we train five models (same architecture, different seeds) and require that all models predict an object to qualify as a pseudo label. Unlike Mix-Teaching

[23], which uses the most confident model for pseudo annotations, we incorporate all predictions and merge them using a KDE with MLE. We use separate KDEs for x, y, z, w, h , and l and employ s_{pseudo} as the KDE weight. As in previous work [43], we take the rotation prediction from the most confident teacher. We prefer a KDE for robustness to noise over methods like WBF [52], as used in SOAP [42].

F. Diversity Maximization (DM)

With the above three stages, we can identify high-quality pseudo labels for self-training by enforcing a threshold $s_{\text{pseudo}} > s_{\text{min}}$. However, we observe a tendency for specific configurations, such as cars driving forward, backward, left, or right relative to the camera, to be selected more frequently as pseudo labels. This pattern likely arises because these orientations are more prevalent in the dataset. Unfortunately, this can result in oversampling and introduce a bias toward simpler cases.

To address this issue, we propose Diversity Maximization to enhance the rotation variety of pseudo labels. Let R_1, \dots, R_n denote the allocentric [49] rotation matrices of the merged pseudo labels. We first measure the diversity of a pseudo label i with rotation matrix R_i w.r.t. the $N = 2,500$ most confident pseudo labels we would have chosen without diversity maximization. We can use the geodesic distance d_{geo} as it measures the shortest path between two rotations on the $SO(3)$ rotation manifold:

$$d_{\text{geo}}(R_1, R_2) = \|\log(R_1^T R_2)\|. \quad (7)$$

However, this approach encourages opposing directions, which lead to the maximum distance and are not desirable in our context. To address this, we employ the following recalibrated version with $n_c = 2$, which results in diversity peaks when being at a distance of 45° and 135° wrt. the average orientation:

$$d_{\text{recalib}}(R_1, R_2) = \min \left(d, \frac{\pi}{n_c} - d \right) \text{ with} \quad (8)$$

$$d = \frac{d_{\text{geo}}(R_1, R_2)}{\sqrt{2}} \text{ mod } \frac{\pi}{n_c}.$$

Our diversity score is then defined as:

$$s_{\text{div}} = \frac{1}{N-1} \sum_{j \neq i} d_{\text{recalib}}(R_i, R_j) \cdot \frac{n_c}{\pi}. \quad (9)$$

We rank the pseudo labels using the formula $(1 - w_{\text{div}}) \cdot \bar{s}_{\text{pseudo}} + w_{\text{div}} \cdot s_{\text{div}}$, where \bar{s}_{pseudo} is the average \bar{s}_{pseudo} score across all 5 teacher models. We then select the top N objects as final pseudo labels for self-training. In our experiments, we set $w_{\text{div}} = 0.2$.

IV. EXPERIMENTS

Implementation Details Our MonoCT uses DLA-34 [54] as the backbone, conducted on a single NVIDIA A40. We utilize the AdamW optimizer [55] with a cosine learning rate scheduler, setting the learning rate to 2.25×10^{-4} and weight decay to 10^{-5} . We paste up to 8 pseudo labels per image.

TABLE I: **Domain adaptation results for dataset shifts (real)**. Results are shown for the car class. MCVD* denotes MonoCon [35] with Virtual Depth [49].

Method	AP _{BEV} ⁵⁰			AP _{3D} ⁵⁰		
	Easy	Mod	Hard	Easy	Mod	Hard
nuScenes [56] → KITTI [27], R40						
Oracle	64.86	49.17	44.35	60.81	45.72	39.96
STMono3D [21]	35.63	23.62	22.18	29.01	19.88	17.17
DGMono3D [20]	34.22	28.99	27.82	28.77	24.82	23.67
MonoGDG [19]	39.50	32.39	32.07	33.48	27.14	26.37
MCVD* (Baseline)	32.96	23.98	20.02	21.31	14.89	17.36
MonoCT (Ours)	52.39	36.24	34.95	42.80	32.24	27.36
Lyft [48] → KITTI [27], R11						
Oracle	62.16	51.59	45.76	62.16	46.21	43.33
STMono3D [21]	26.46	20.71	11.83	18.14	13.32	11.83
DGMono3D [20]	36.18	28.30	22.23	30.03	23.28	22.23
MonoGDG [19]	38.47	30.89	29.58	32.48	26.02	24.96
MCVD* (Baseline)	37.59	27.21	25.15	31.27	23.97	20.34
MonoCT (Ours)	59.54	43.70	38.07	50.54	36.33	30.50

TABLE II: **Domain generalization results for dataset shifts (synthetic + real)**: nuScenes [56] + PreSIL [57] → KITTI [27]. Results are shown for the car class (R40).

Method	AP _{BEV} ⁵⁰			AP _{3D} ⁵⁰		
	Easy	Mod	Hard	Easy	Mod	Hard
Oracle	64.86	49.17	44.35	60.81	45.72	39.96
STMono3D [21]	32.47	23.35	19.81	24.43	17.37	14.29
DGMono3D [20]	33.81	27.27	26.84	24.75	20.08	19.58
MonoGDG [19]	38.35	29.48	28.71	31.55	23.31	22.25
MCVD* (Baseline)	31.16	21.26	18.32	23.99	16.96	13.72
MonoCT (Ours)	56.45	35.62	28.83	49.44	30.33	25.12

A. Cross Dataset Domain Adaptation

We evaluate our MonoCT on the benchmarks [21], [19] for domain adaptation, which includes cross-dataset adaptation, synthetic-to-real transfer, and adaptation to various weather conditions. To ensure fairness, we exclude validation images from the unlabeled set, leaving 39,522 KITTI images.

We train separately on NuScenes (204,894 images, Boston and Singapore) [56] and Lyft (136,080 images, Palo Alto) [48], evaluating on KITTI val. (3,769 images, Germany) [27]. Both NuScenes and Lyft are subsampled to 1/4 of their data as in prior work [21]. We report AP_{BEV} and AP_{3D} at an IoU of 0.5 for the car class (see Table I). We establish an oracle baseline by training MonoCon [35] directly on the target dataset. Training exclusively on source data yields significantly degraded performance, highlighting the vulnerability of current state-of-the-art methods to cross-dataset domain shifts. Our approach effectively reduces this domain gap, retaining over 96%, 85%, and 83% of the oracle performance on Lyft [48] → KITTI [27] AP_{BEV}. These results confirm that our method adapts 3D object detectors to the target domain more effectively and significantly outperforms existing methods. Notice that our method does not increase inference time, as it is only used to generate better labels for self-supervision.

We then perform joint training on NuScenes [56] and the

TABLE III: **Domain adaptation results for dataset and weather shifts**: NuScenes [56] + PreSIL [57] → KITTI fog/rain [58], [59]. Results are shown in AP_{3D}⁵⁰ R40 for cars.

Method	KITTI fog [58] AP _{3D} ⁵⁰			KITTI rain [59]		
	Easy	Mod	Hard	Easy	Mod	Hard
Oracle	60.55	44.14	39.56	61.08	44.42	39.70
STMono3D [21]	19.59	14.63	13.35	23.18	16.46	13.59
DGMono3D [20]	17.64	12.52	11.84	22.30	15.92	15.26
MonoGDG [19]	23.58	15.97	15.28	27.69	18.33	17.79
MCVD* (Baseline)	13.91	9.60	8.07	14.63	11.41	10.01
MonoCT (Ours)	39.18	23.88	18.28	41.55	25.52	19.63

TABLE IV: MonoCT improves detection accuracy on the traffic- and drone-view datasets. Results are reported for Car.

Method	Rope3D [8] AP _{3D} ⁷⁰	CDrone [9] AP _{3D} ⁵⁰
MCVD* (Baseline)	4.73	8.91
MonoCT (Ours)	6.47	13.63
Improvement	+ 36.8%	+ 53.0%

synthetic dataset PreSIL (51,075 images, GTA V) [57], and evaluate on KITTI val. [27] (*cf.* Table II). Our MonoCT performs consistently better than previous SOTA networks for the easy, moderate, and hard categories.

Additionally, we test generalization under different weather conditions. Training on NuScenes [56] and PreSIL [57], we evaluate on KITTI val. rain [59] and KITTI val fog [58] (*cf.* Table III). The baseline accuracy drops by 43.3% and 32.7%, whereas our approach only decreases by 21.3% and 15.9% for AP Mod. Notably, fog and rain images constitute less than 10% of the unlabeled data here, as only the KITTI trainval set is provided with fog/rain [58], [59]. Despite this limitation, our MonoCT significantly outperforms previous methods and the baseline, demonstrating its robustness and generalizability.

B. Domain adaptation for traffic- and drone-view datasets

We evaluate MonoCT on static camera datasets, Rope3D (traffic-view dataset with 45,008 images) [8] and CDrone (drone-view dataset with 37,800 images) [9], both of which have cameras at a limited number of locations only. This makes it difficult to generalize to new camera locations when the training and test sets are from different locations [13], [60]. To overcome this, we use sufficient unlabeled images from the test locations to boost accuracy.

Due to the limited images in raw test sets for Rope3D, we combine the raw training and validation set and sample half the locations for training. The remaining images are evenly divided between unlabeled data and evaluation sets, ensuring both contain the same locations. For CDrone, the training set serves as source data, and the combined validation and test set represents the target data, designating the first half of each video sequence as unlabeled. The last 25% are used as test data, again ensuring both sets share the same locations. Results in Table IV show a 36.8% improvement on Rope3D and a 53.0% improvement on CDrone, demonstrating the effectiveness of our MonoCT when leveraging unlabeled data for diverse camera perspectives. Notably, pre-training

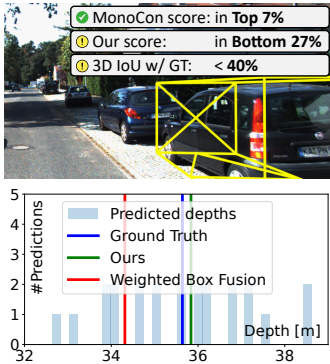


Fig. 4: **Top**: PLS filters inaccurate pseudo labels better than default scoring. **Bottom**: KDE-based depth merging is more robust to outliers than WBF [52].

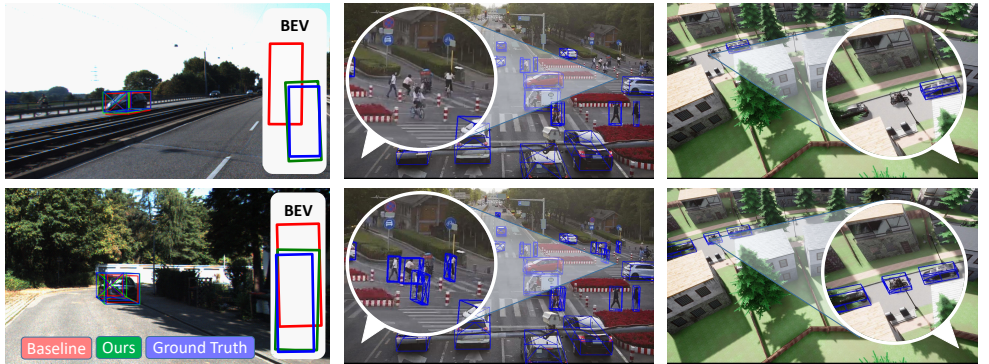


Fig. 5: **Qualitative Results.** Lyft [48] \rightarrow KITTI [27] (Column 1): Our pseudo label supervision allows MonoCT to predict depth more accurately than MonoCon [35], as evident in the *bird's-eye view* (BEV) visualization. **Rope3D** [8] and **CDrone** [9] (Columns 2 and 3): We compare our baseline MonoCon [35] (row 1) with MonoCT (row 2). MonoCT demonstrates superior detection of occluded and distant objects in new environments.

TABLE V: **Ablation Study:** Lyft [48] \rightarrow KITTI [27]. We individually remove each component (**bold**) and sub-component from MonoCT and report AP_{3D}^{50} in R11 for Car.

Method	Easy	Mod	Hard
MonoCT (Ours)	50.54	36.33	30.49
w/o Generalized Depth Enhancement (GDE)	36.17	26.40	23.91
w/o Keypoint to depth	42.70	31.79	26.03
w/o 2D bbox to depth	43.53	32.49	27.68
w/ Weighted Box Fusion (WBF) [52], [26]	39.69	27.57	21.69
w/o Pseudo Label Scoring (PLS)	41.02	30.73	26.82
w/o 2D/3D BBox consistency score	47.27	34.61	29.37
w/ Mix-Teaching [23] ensemble score	42.83	31.33	25.95
w/o Ensemble Merging (EM)	46.99	32.61	26.11
w/o Diversity Maximization (DM)	43.19	28.50	25.68

on other datasets yielded no significant empirical benefits.

C. Ablation Study

We validate the effectiveness of our MonoCT by systematically removing each component on the Lyft [48] \rightarrow KITTI [27] benchmark (*cf.* Table V). Among the primary components, GDE proves to be the most influential. Removing its subcomponents *keypoint-to-depth* or *2D-bounding-box-to-depth* results in a 12.5% and 10.6% reduction in AP_{3D} Mod, respectively, underscoring the necessity of incorporating both elements together. However, these additional depth estimates introduce significant outliers, which likely explains the 24.1% performance drop in the Mod category when using a weighted average for fusion instead of a KDE with MLE (*cf.* Fig. 4 for a concrete example). Replacing PLS by the default score in MonoCon or with the ensemble score in Mix-Teaching reduces accuracy by 15.4% and 13.8% respectively (*cf.* example in Fig. 4), while removing the 2D/3D BBox consistency subscore reduces prediction quality by 4.7%. To further validate our choice of pseudo label score, we compute the Spearman Rank Correlation between various scoring methods and the ground truth on the top 10% of labels. Our pseudo label score achieves a correlation of 0.40, outperforming both the default MonoCon score (0.31) and the Mix-Teaching 3D IoU ensemble score (0.24). Removing *Ensemble*

Merging (EM) results in a 10.2% decrease in accuracy, highlighting that combining multiple teacher predictions is more effective than relying solely on the most confident prediction, as in Mix-Teaching [23]. Lastly, eliminating DM results in a 21.6% decrease in AP_{3D} Mod, confirming the critical role of enhancing pseudo-label quality and diversity. The effect of this enhancement is further illustrated in Fig. 3, which demonstrates the increased variety of pseudo labels achieved with Diversity Maximization.

D. Qualitative Results

In Fig. 5, we present qualitative comparisons of our baseline MonoCon [35] and MonoCT. For Lyft [48] \rightarrow KITTI [27], MonoCT demonstrates more accurate depth predictions. This improvement is expected, as MonoCT performs self-training on a carefully selected subset of pseudo labels, which underwent both single-model depth enhancement through GDE and multi-model enhancement via *EM*. Additionally, MonoCT excels at detecting more objects in new camera locations for Rope3D [8] and CDrone [9] (see experimental setup in Section IV-B).

V. CONCLUSION

We introduce MonoCT, a carefully designed method to handle domain shift in monocular 3D object detection. MonoCT first converts auxiliary 2D predictions into depth estimates, significantly improving depth accuracy. Second, it enhances pseudo label scoring by incorporating model consistency measures. Third, MonoCT optimizes for both label quality and diversity to boost generalization. Experimental results demonstrate that MonoCT significantly improves detection accuracy over existing methods. Additionally, MonoCT shows superior generalization to new camera locations, underscoring its robustness and adaptability across diverse camera views.

Limitations Our evaluation is limited to outdoor scenes. While MonoCT's components could theoretically apply to tasks like semi-supervised learning, few-shot learning, and general monocular 3D detection, we have not evaluated these applications yet. We plan to explore this in future work.

REFERENCES

- [1] Y. Xia, Y. Xu, C. Wang, and U. Stilla, "Vpc-net: Completion of 3d vehicles from mls point clouds," *ISPRS Journal of Photogrammetry and Remote Sensing*, vol. 174, pp. 166–181, 2021.
- [2] Y. Shan, Y. Xia, Y. Chen, and D. Cremers, "Scp: Scene completion pre-training for 3d object detection," *The International Archives of the Photogrammetry, Remote Sensing and Spatial Information Sciences*, vol. 48, pp. 41–46, 2023.
- [3] Y. Chen, J. Liu, X. Zhang, X. Qi, and J. Jia, "Largekernel3d: Scaling up kernels in 3d sparse cnns," in *Conference on Computer Vision and Pattern Recognition, CVPR*, 2023, pp. 13 488–13 498.
- [4] Y. Chen, Z. Yu, Y. Chen, S. Lan, A. Anandkumar, J. Jia, and J. M. Álvarez, "Focalformer3d : Focusing on hard instance for 3d object detection," in *International Conference on Computer Vision, ICCV*, 2023, pp. 8360–8371.
- [5] Y. Xia, Q. Wu, W. Li, A. B. Chan, and U. Stilla, "A lightweight and detector-free 3d single object tracker on point clouds," *IEEE Transactions on Intelligent Transportation Systems*, vol. 24, no. 5, pp. 5543–5554, 2023.
- [6] O. Wysocki, Y. Xia, M. Wysocki, E. Grilli, L. Hoegner, D. Cremers, and U. Stilla, "Scan2lod3: Reconstructing semantic 3d building models at lod3 using ray casting and bayesian networks," in *Proceedings of the IEEE/CVF Conference on Computer Vision and Pattern Recognition*, 2023, pp. 6548–6558.
- [7] H. Yu, Y. Luo, M. Shu, Y. Huo, Z. Yang, Y. Shi, Z. Guo, H. Li, X. Hu, J. Yuan, and Z. Nie, "DAIR-V2X: A large-scale dataset for vehicle-infrastructure cooperative 3D object detection," in *Conference on Computer Vision and Pattern Recognition, CVPR*, 2022, pp. 21 329–21 338.
- [8] X. Ye, M. Shu, H. Li, Y. Shi, Y. Li, G. Wang, X. Tan, and E. Ding, "Rope3D: The roadside perception dataset for autonomous driving and monocular 3D object detection task," in *Conference on Computer Vision and Pattern Recognition, CVPR*, 2022, pp. 21 309–21 318.
- [9] J. Meier, L. Scalerandi, O. Dhauadi, J. Kaiser, A. Nikita, and D. Cremers, "CARLA Drone: monocular 3d object detection from a different perspective," in *German Conference on Pattern Recognition, GCPR*, 2024.
- [10] H. Yu, W. Yang, H. Ruan, Z. Yang, Y. Tang, X. Gao, X. Hao, Y. Shi, Y. Pan, N. Sun, J. Song, J. Yuan, P. Luo, and Z. Nie, "V2x-seq: A large-scale sequential dataset for vehicle-infrastructure cooperative perception and forecasting," in *Conference on Computer Vision and Pattern Recognition, CVPR*, 2023, pp. 5486–5495.
- [11] R. Krajewski, J. Bock, L. Kloeker, and L. Eckstein, "The highd dataset: A drone dataset of naturalistic vehicle trajectories on german highways for validation of highly automated driving systems," in *International Conference on Intelligent Transportation Systems, ITSC*, 2018, pp. 2118–2125.
- [12] J. Bock, R. Krajewski, T. Moers, S. Runde, L. Vater, and L. Eckstein, "The ind dataset: A drone dataset of naturalistic road user trajectories at german intersections," in *Intelligent Vehicles Symposium, IV*, 2020, pp. 1929–1934.
- [13] H. Shi, C. Pang, J. Zhang, K. Yang, Y. Wu, H. Ni, Y. Lin, R. Stiefel-hagen, and K. Wang, "Cobev: Elevating roadside 3d object detection with depth and height complementarity," *CoRR*, 2023.
- [14] Z. Li, W. Wang, H. Li, E. Xie, C. Sima, T. Lu, Y. Qiao, and J. Dai, "Bevformer: Learning bird's-eye-view representation from multi-camera images via spatiotemporal transformers," in *European Conference on Computer Vision, ECCV*, vol. 13669, 2022, pp. 1–18.
- [15] D. Tsai, J. S. Berrio, M. Shan, E. M. Nebot, and S. Worrall, "Viewer-centred surface completion for unsupervised domain adaptation in 3d object detection," in *International Conference on Robotics and Automation, ICRA*, 2023, pp. 9346–9353.
- [16] D. Hegde, V. Kilic, V. Sindagi, A. B. C. III, M. A. Foster, and V. M. Patel, "Source-free unsupervised domain adaptation for 3d object detection in adverse weather," in *International Conference on Robotics and Automation, ICRA*, 2023, pp. 6973–6980.
- [17] Y. You, C. A. Diaz-Ruiz, Y. Wang, W.-L. Chao, B. Hariharan, M. Campbell, and K. Q. Weinberger, "Exploiting playbacks in unsupervised domain adaptation for 3d object detection in self-driving cars," in *2022 International Conference on Robotics and Automation (ICRA)*, 2022, pp. 5070–5077.
- [18] S. Chen, B. Yang, Y. Xia, M. Cheng, S. Shen, and C. Wang, "Bridging lidar gaps: A multi-lidars domain adaptation dataset for 3d semantic segmentation," in *Proceedings of the Thirty-Third International Joint Conference on Artificial Intelligence, IJCAI-24*, 2024, pp. 650–658.
- [19] F. Yang, H. Chen, Y. He, S. Zhao, C. Zhang, K. Ni, and G. Ding, "Geometry-guided domain generalization for monocular 3d object detection," in *Conference on Artificial Intelligence, AAAI*. AAAI Press, 2024, pp. 6467–6476.
- [20] L. Zhenyu, C. Zehui, L. Ang, F. Liangji, Q. Jiang, L. Xianming, and J. Junjun, "Towards model generalization for monocular 3d object detection," *CoRR*, vol. abs/2205.11664, 2022.
- [21] Z. Li, Z. Chen, A. Li, L. Fang, Q. Jiang, X. Liu, and J. Jiang, "Unsupervised domain adaptation for monocular 3d object detection via self-training," in *European Conference on Computer Vision, ECCV*, vol. 13669, 2022, pp. 245–262.
- [22] H. Lin, Y. Zhang, S. Niu, S. Cui, and Z. Li, "Fully test-time adaptation for monocular 3d object detection," *CoRR*, 2024.
- [23] L. Yang, X. Zhang, J. Li, L. Wang, M. Zhu, C. Zhang, and H. Liu, "Mix-Teaching: A simple, unified and effective semi-supervised learning framework for monocular 3D object detection," *IEEE Trans. Circuits Syst. Video Technol.*, vol. 33, no. 11, pp. 6832–6844, 2023.
- [24] Y. Zhang, J. Lu, and J. Zhou, "Objects are different: Flexible monocular 3D object detection," in *Conference on Computer Vision and Pattern Recognition, CVPR*, 2021, pp. 3289–3298.
- [25] L. Yan, P. Yan, S. Xiong, X. Xiang, and Y. Tan, "Monocd: Monocular 3d object detection with complementary depths," in *Conference on Computer Vision and Pattern Recognition, CVPR*, 2024, pp. 10 248–10 257.
- [26] Z. Li, Z. Qu, Y. Zhou, J. Liu, H. Wang, and L. Jiang, "Diversity matters: Fully exploiting depth clues for reliable monocular 3D object detection," in *Conference on Computer Vision and Pattern Recognition, CVPR*, 2022, pp. 2781–2790.
- [27] A. Geiger, P. Lenz, and R. Urtasun, "Are we ready for autonomous driving? The KITTI vision benchmark suite," in *Conference on Computer Vision and Pattern Recognition, CVPR*, 2012, pp. 3354–3361.
- [28] P. Sun, H. Kretschmar, X. Dotiwalla, A. Chouard, V. Patnaik, P. Tsui, J. Guo, Y. Zhou, Y. Chai, B. Caine, V. Vasudevan, W. Han, J. Ngiam, H. Zhao, A. Timofeev, S. Ettinger, M. Krivokon, A. Gao, A. Joshi, Y. Zhang, J. Shlens, Z. Chen, and D. Anguelov, "Scalability in perception for autonomous driving: Waymo open dataset," in *Conference on Computer Vision and Pattern Recognition, CVPR*, 2020, pp. 2443–2451.
- [29] Z. Qin and X. Li, "Monoground: Detecting monocular 3d objects from the ground," in *Conference on Computer Vision and Pattern Recognition, CVPR*. IEEE, 2022, pp. 3783–3792.
- [30] Z. Wu, Y. Gan, L. Wang, G. Chen, and J. Pu, "Monopgc: Monocular 3d object detection with pixel geometry contexts," in *IEEE International Conference on Robotics and Automation, ICRA 2023, London, UK, May 29 - June 2, 2023*, 2023, pp. 4842–4849.
- [31] D. Park, J. Li, D. Chen, V. Guizilini, and A. Gaidon, "Depth is all you need for monocular 3d detection," in *International Conference on Robotics and Automation, ICRA*, 2023, pp. 7024–7031.
- [32] A. Kumar, G. Brazil, E. Corona, A. Parchami, and X. Liu, "Deviant: Depth equivariant network for monocular 3D object detection," in *European Conference on Computer Vision, ECCV*, 2022, pp. 664–683.
- [33] Z. Li, J. Jia, and Y. Shi, "Monolss: Learnable sample selection for monocular 3d detection," in *International Conference on 3D Vision, 3DV*, 2024, pp. 1125–1135.
- [34] P. Li, H. Zhao, P. Liu, and F. Cao, "RTM3D: real-time monocular 3d detection from object keypoints for autonomous driving," in *European Conference on Computer Vision, ECCV*, vol. 12348, 2020, pp. 644–660.
- [35] X. Liu, N. Xue, and T. Wu, "Learning auxiliary monocular contexts helps monocular 3D object detection," in *Conference on Artificial Intelligence, AAAI*, 2022, pp. 1810–1818.
- [36] M. K. Wozniak, M. Hansson, M. Thiel, and P. Jensfelt, "UADA3D: unsupervised adversarial domain adaptation for 3d object detection with sparse lidar and large domain gaps," *CoRR*, vol. abs/2403.17633, 2024.
- [37] Y. Zhang, C. Zhou, and D. Huang, "Stal3d: Unsupervised domain adaptation for 3d object detection via collaborating self-training and adversarial learning," *IEEE Transactions on Intelligent Vehicles*, pp. 1–12, 2024.
- [38] Y.-J. Li, M. Gladkova, Y. Xia, R. Wang, and D. Cremers, "Vxp: Voxel-cross-pixel large-scale image-lidar place recognition," *arXiv preprint arXiv:2403.14594*, 2024.
- [39] Z. Luo, Z. Cai, C. Zhou, G. Zhang, H. Zhao, S. Yi, S. Lu, H. Li, S. Zhang, and Z. Liu, "Unsupervised domain adaptive 3d detection

- with multi-level consistency,” in *International Conference on Computer Vision, ICCV*, 2021, pp. 8846–8855.
- [40] Z. Zhang, M. Chen, S. Xiao, L. Peng, H. Li, B. Lin, P. Li, W. Wang, B. Wu, and D. Cai, “Pseudo label refinery for unsupervised domain adaptation on cross-dataset 3d object detection,” in *Conference on Computer Vision and Pattern Recognition, CVPR*, 2024.
- [41] D. Tsai, J. S. Berrio, M. Shan, E. M. Nebot, and S. Worrall, “MS3D++: ensemble of experts for multi-source unsupervised domain adaption in 3d object detection,” *CoRR*, vol. abs/2308.05988, 2023.
- [42] C. Huang, V. Abdelzad, S. Sedwards, and K. Czarniecki, “SOAP: cross-sensor domain adaptation for 3d object detection using stationary object aggregation pseudo-labelling,” in *Winter Conference on Applications of Computer Vision, WACV*, 2024, pp. 3340–3349.
- [43] D. Tsai, J. S. Berrio, M. Shan, E. M. Nebot, and S. Worrall, “MS3D: leveraging multiple detectors for unsupervised domain adaptation in 3d object detection,” in *International Conference on Intelligent Transportation Systems, ITSC*, 2023, pp. 140–147.
- [44] J. Liu, R. Zhang, X. Li, X. Chi, Z. Chen, M. Lu, Y. Guo, and S. Zhang, “BEVUDA: multi-geometric space alignments for domain adaptive BEV 3d object detection,” in *IEEE International Conference on Robotics and Automation, ICRA 2024, Yokohama, Japan, May 13-17, 2024*, 2024, pp. 9487–9494.
- [45] X. Li, J. Liu, Y. Lei, L. Ma, X. Fan, and R. Liu, “Monotdp: Twin depth perception for monocular 3d object detection in adverse scenes,” *CoRR*, 2023.
- [46] L. Zheng, Y. Liu, Y. Wang, and H. Zhao, “Cross-dataset sensor alignment: Making visual 3d object detector generalizable,” in *Conference on Robot Learning, CoRL*, vol. 229, 2023, pp. 1903–1929.
- [47] X. Zhou, D. Fu, W. Zimmer, M. Liu, V. Lakshminarasimhan, L. Strand, and A. Knoll, “Warm-3d: A weakly-supervised sim2real domain adaptation framework for roadside monocular 3d object detection,” in *International Intelligent Transportation Systems Conference, ITSC*, 2024.
- [48] G. Li, Y. Jiao, V. L. Knoop, S. C. Calvert, and J. W. C. van Lint, “Large car-following data based on lyft level-5 open dataset: Following autonomous vehicles vs. human-driven vehicles,” in *International Conference on Intelligent Transportation Systems, ITSC*, 2023, pp. 5818–5823.
- [49] G. Brazil, A. Kumar, J. Straub, N. Ravi, J. Johnson, and G. Gkioxari, “Omni3D: A large benchmark and model for 3D object detection in the wild,” in *Conference on Computer Vision and Pattern Recognition, CVPR*, 2023, pp. 13 154–13 164.
- [50] H. Zhang, M. Cissé, Y. N. Dauphin, and D. Lopez-Paz, “mixup: Beyond empirical risk minimization,” in *International Conference on Learning Representations, ICLR*, 2018.
- [51] Y. Lu, X. Ma, L. Yang, T. Zhang, Y. Liu, Q. Chu, J. Yan, and W. Ouyang, “Geometry uncertainty projection network for monocular 3D object detection,” in *International Conference on Computer Vision, ICCV*, 2021, pp. 3091–3101.
- [52] R. A. Solovyev, W. Wang, and T. Gabruseva, “Weighted boxes fusion: Ensembling boxes from different object detection models,” *Image Vis. Comput.*, vol. 107, p. 104117, 2021.
- [53] B. W. Silverman, *Density Estimation for Statistics and Data Analysis*. Springer, 1986.
- [54] F. Yu, D. Wang, E. Shelhamer, and T. Darrell, “Deep layer aggregation,” in *Conference on Computer Vision and Pattern Recognition, CVPR*, 2018.
- [55] I. Loshchilov and F. Hutter, “Decoupled weight decay regularization,” in *International Conference on Learning Representations, ICLR*, 2019.
- [56] H. Caesar, V. Bankiti, A. H. Lang, S. Vora, V. E. Liong, Q. Xu, A. Krishnan, Y. Pan, G. Baldan, and O. Beijbom, “NuScenes: A multimodal dataset for autonomous driving,” in *Conference on Computer Vision and Pattern Recognition, CVPR*, 2020, pp. 11 618–11 628.
- [57] B. Hurl, K. Czarniecki, and S. L. Waslander, “Precise synthetic image and lidar (presil) dataset for autonomous vehicle perception,” in *Intelligent Vehicles Symposium, IV*. IEEE, 2019, pp. 2522–2529.
- [58] N. A. M. Mai, P. Duthon, L. Khoudour, A. Crouzil, and S. A. Velastin, “3d object detection with sls-fusion network in foggy weather conditions,” *Sensors*, vol. 21, no. 20, p. 6711, 2021.
- [59] S. S. Halder, J. Lalonde, and R. de Charette, “Physics-based rendering for improving robustness to rain,” in *International Conference on Computer Vision, ICCV*. IEEE, 2019, pp. 10 202–10 211.
- [60] X. Chen, M. Chen, S. Tang, Y. Niu, and J. Zhu, “MOSE: Boosting vision-based roadside 3D object detection with scene cues,” *arXiv:2404.05280 [cs.CV]*, 2024.